

ELECTROMAGNETIC TRANSIENTS POWERED BY NUCLEAR DECAY IN THE TIDAL TAILS OF COALESCING COMPACT BINARIES

L. F. ROBERTS¹, D. KASEN^{2,3}, W. H. LEE⁴, AND E. RAMIREZ-RUIZ¹

Draft version July 10, 2018

ABSTRACT

The possibility that long tidal tails formed during compact object mergers may power optical transients through the decay of freshly synthesized r -process material is investigated. Precise modeling of the merger dynamics allows for a realistic determination of the thermodynamic conditions in the ejected debris. The results of hydrodynamic and full nuclear network calculations are combined to calculate the resultant r -process abundances and the heating of the material by their decays. The subsequent homologous structure is mapped into a radiative transfer code to synthesize emergent model light curves and determine how their properties (variability and color evolution) depend on the mass ratio and orientation of the merging binary. The radiation emanating from the ejected debris, though less spectacular than a typical supernova, should be observable in transient surveys and we estimate the associated detection rates. The case for (or against) compact object mergers as the progenitors of short gamma-ray bursts can be tested if such electromagnetic transients are detected (or not) in coincidence with some bursts, although they may be obscured by on-axis afterglows.

Subject headings: nuclear reactions, nucleosynthesis, abundances — black hole physics — radiative transfer — stars: neutron — hydrodynamics — gamma-ray burst: general

1. INTRODUCTION

Merging compact binaries are the primary candidate for direct detection of gravitational waves (GWs) by LIGO (Abbott et al. 2008), and are thought to be the progenitors of short gamma-ray bursts (SGRBs) (c.f. Lee & Ramirez-Ruiz 2007; Rosswog 2007; Nakar 2007; Gehrels et al. 2009). Current observational limits indicate that any supernova-like event accompanying SGRBs would have to be over 50 times fainter than normal Type Ia SNe or Type Ic supernovae (SNe), (Hjorth et al. 2005; Bloom et al. 2006). These limits strongly constrain progenitor models for SGRBs (Lee & Ramirez-Ruiz 2007; Perley et al. 2009; Kocevski et al. 2010). Unless SGRBs are eventually found to be accompanied by telltale optical signatures like the supernovae of long-duration GRBs (Hjorth et al. 2003), the only definitive understanding of the progenitors will come from possible associations to direct gravitational or neutrino signals (Rosswog & Liebendörfer 2003).

The merger of compact objects does not necessarily imply the absence of optical or other long-wavelength phenomena after coalescence. Neutron-rich material may be dynamically ejected during a NS-NS (Neutron Star) or a NS-BH (Black Hole) merger. Material dynamically stripped from a star is violently ejected by tidal torques through the outer Lagrange point, removing energy and angular momentum and forming a large tidal tail. Its subsequent decompression may synthesize radioactive elements through the r -process (Lattimer &

Schramm 1976; Freiburghaus et al. 1999), whose radioactive decay could power an optical transient (Li & Paczyński 1998; Metzger et al. 2010b). For double NS binaries there are one or two such structures, depending on the mass ratio and equation of state (EoS) of the NSs (Oechslin et al. 2007). Clearly, only one tail (or no tail) is formed in a BH-NS merger, and these are typically a few thousand kilometers in size by the end of the disruption event and some of the fluid (as much as a few hundredths of a solar mass) is often gravitationally unbound.

The most efficient conversion of radioactive energy to radiation is provided by those isotopes with a decay timescale comparable to the radiative diffusion time through the ejecta. In reality, there are likely to be a large number of nuclides with a very broad range of decay timescales (Li & Paczyński 1998; Metzger et al. 2010b). Current observational limits thus place interesting constraints on the nuclear evolution of this material, as well as the total mass ejected in these events.

In this *Letter*, we present the results of multi-dimensional hydrodynamics simulations of neutron star mergers for various binary mass ratios. The ejected material is then post-processed with a full nuclear network and a radiation transport code. Our goal here is to investigate how radioactive r -process elements synthesized in the tidal tails could power electromagnetic transients and how their properties may depend on the mass ratio of the merging binary. We also discuss prospects for detection and implications for SGRBs.

2. TIDAL TAIL EVOLUTION

2.1. Ejection

To calculate the ejected mass and structure of the tidal tails, we employ a three dimensional smoothed particle hydrodynamics (SPH) method to compute the evolution of the compact object merger (Lee & Ramirez-Ruiz 2007; Lee et al. 2010). Due to its Lagrangian

¹ Department of Astronomy and Astrophysics, University of California, Santa Cruz, CA 95064 USA

² Departments of Physics and Astronomy, University of California, Berkeley, 94270, USA

³ Nuclear Science Division, Lawrence Berkeley National Laboratory, Berkeley, CA, 94720, USA

⁴ Instituto de Astronomía, Universidad Nacional Autónoma de México, Apdo. Postal 70-264, Cd. Universitaria, México DF 04510

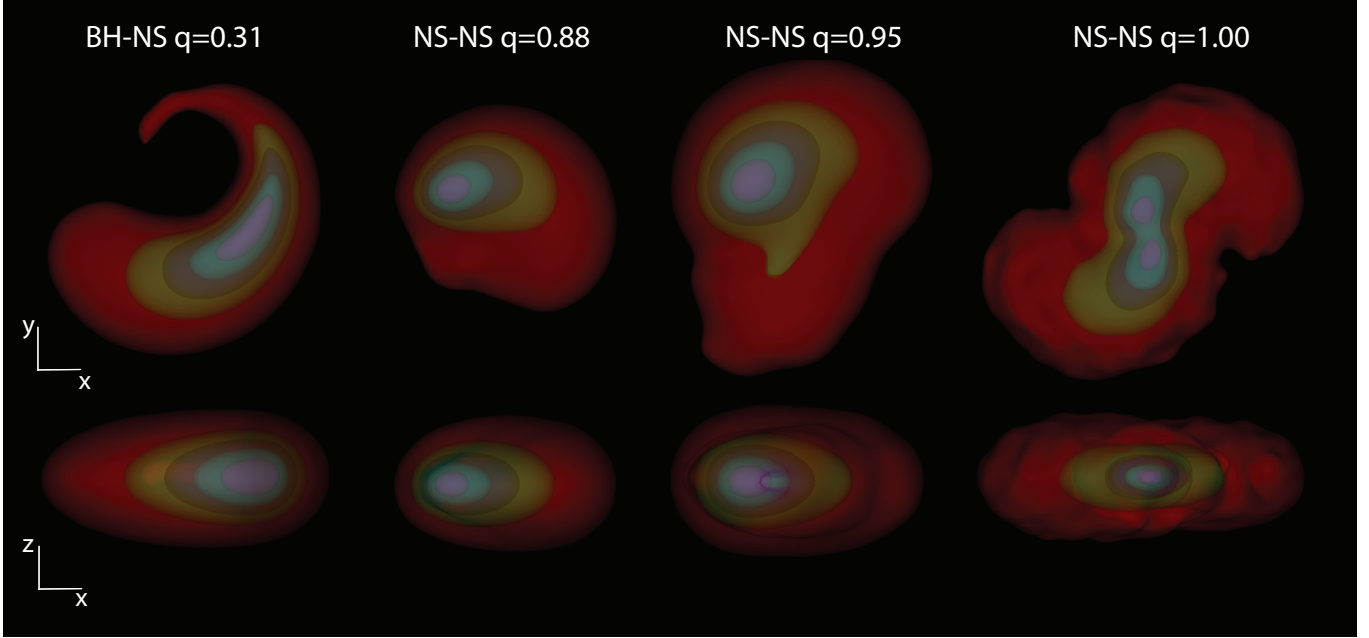


Figure 1. Homologous structure of ejected material in the four models considered in this work (see table 1) viewed face on (top) and edge on (bottom). The density contours are not the same between models, we have instead chosen to plot the models at the same size scale. The peak density contour (blue) is twenty times the minimum density contour (red). The evolution from one to two tidal tails in the NS-NS mergers as the mass ratio approaches unity is clearly visible.

nature, SPH is perfectly suited to follow tidal disruption processes during which the corresponding geometry, densities, and time scales are changing violently (c.f. Rasio & Shapiro 1994; Lee 2000; Rosswog et al. 2003). The equation of state is a hybrid, where we have combined the cold Friedman-Pandharipande-Skyrme (FPS) nuclear EoS with an ideal thermal component as described by Shibata et al. (2005). Once the fluid in the tidal tails has become unbound, the full SPH calculations are stopped and the particles are followed on ballistic trajectories in the potential of the central compact remnant until their expansion becomes homologous.

To explore the possible range of outcomes depending on the physical parameters of the binary system, we have considered four models: three NS-NS mergers with mass ratios $q = M_2/M_1 = 1, 0.95, 0.88$ and one BH-NS merger with $q = 0.31$. Around $0.05M_\odot$ of material is ejected in all four models. Relevant parameters resulting from the simulations are given in table 1. The density structure of the tails is shown in figure 1 at homology. Clearly, there is a progression from equal mass tails in the $q = 1.0$ case to almost no secondary tail in the $q = 0.88$ NS-NS case. The relative mass of the two tails is a function of the mass ratio and the nature of the merging objects, as well as the underlying EoS (which we have not explored in this work). It is of interest to determine if different tail geometries are distinguishable in the optical signal from a compact object merger, as this would provide a significant constraint on the nature of the objects involved in addition to the expected gravitational wave signal.

2.2. Nuclear Evolution

We follow the evolution of the composition of the tails using a 6312 isotope nuclear reaction network which extends past Uranium. Density histories of particles from

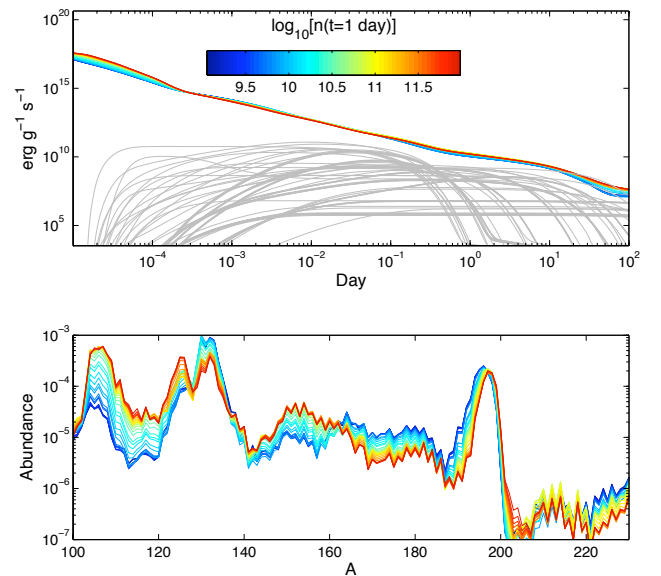


Figure 2. Top: energy deposition rate from nuclear decay (including neutrino losses) as a function of time for various Lagrangian trajectories from the SPH simulations. These are shown for the BH-NS merger, but are representative of the NS-NS mergers as well. The trajectories are color coded by their density one day after the explosion. The gray lines show the heating rate from single reactions that contribute significantly after 0.1 days for a single trajectory. Bottom: final abundances as a function of nuclear mass for the same trajectories.

Table 1
Characteristics of simulations

Type	Mass Ratio	Primary Mass (M_{\odot})	Ejected Mass (M_{\odot})	Ejecta Velocity (c)	t_h^a (s)	t_{peak}^b (days)	t_{dec}^c (days)	L_{peak}^d (erg s^{-1})
NS-NS	1.00	1.4	0.057	0.202	3.2	0.93	1.7	1.51×10^{42}
NS-NS	0.95	1.4	0.047	0.200	2.0	0.93	1.6	1.19×10^{42}
NS-NS	0.88	1.5	0.057	0.205	2.1	1.02	1.8	1.44×10^{42}
BH-NS	0.31	5.4	0.060	0.248	3.9	0.93	1.7	1.64×10^{42}

^a Time to reach 1% deviation from homologous evolution.

^b Time to reach peak bolometric luminosity after merger.

^c Light curve decay timescale.

^d Bolometric Luminosity.

the SPH simulations are employed. The charged particle and neutron capture rates in the network up to At ($Z = 85$) are taken from Rauscher & Thielemann (2000). Past At, the neutron capture rates of Panov et al. (2010) are employed. The network terminates at $Z = 102$. Experimental values are taken for nuclear masses where available, elsewhere theoretical masses are taken from Möller et al. (2003). Neutron induced fission rates are taken from Panov et al. (2010) and the simple approximation of Frankel & Metropolis (1947) is used to calculate spontaneous fission rates. Fission barriers are taken from Mamdouh et al. (2001). For our fission fragment distributions, we employ the empirical fits of Wahl (2002).

The nuclear network is evolved in time using a variant of the code **XNet** (Hix & Thielemann 1999). We have implemented the **PARDISO** sparse matrix solver (Schenk et al. 2008), which makes calculations of large networks with implicitly coupled fission interactions feasible. The energy released by nuclear reactions is self-consistently added back to the material, similar to Freiburghaus et al. (1999).

The material ejected in the tail is from near the surface of the neutron star, making it challenging to determine the initial electron fraction and entropy of the material from our SPH simulations. Therefore, we assume the initial electron fraction to be $Y_e = 0.2$ and start the calculation at $\rho = 10^{11} \text{g cm}^{-3}$ and $T_9 = 1$. The initial composition is then determined by nuclear statistical equilibrium (NSE). As was pointed out by Goriely et al. (2005), if tidally ejected material is un-shocked, the initial temperature of the material is likely much less than our assumed temperature. To test the dependence on the initial temperature, we have run models going down to an initial temperature of $T_9 = 0.2$, and find that the nuclear heating rate is not substantially altered.

The total heating rate and final abundance distribution as a function of mass for a number of fluid elements are shown in figure 2. Similar to Metzger et al. (2010b), we find that the late time heating rate is insensitive to the exact initial conditions and is statistical in nature, as was predicted by Li & Paczyński (1998). At one day, the top five beta-decays contributing to the heating rate are ^{125}Sb , ^{126}Sb , ^{132}I , ^{127}Te , and ^{197}Pt .

2.3. Radiative Transfer

In order to study the radiative transfer problem, we employ the **SEDONA** 3-D time-dependent LTE Monte Carlo radiative transfer code which includes gamma-ray

transfer and spectropolarization (Kasen et al. 2006). The output of the hydrodynamic simulations is mapped into the radiative transfer code and the properties of the emergent radiation are calculated. A global nuclear heating rate based on a fit to the nuclear network calculations is employed. We approximately account for neutrino losses by assuming 75% of the nuclear network energy generation is deposited in the material (Metzger et al. 2010b). Of the energy that is left, we assume 50% is deposited as gamma rays from decays while the other 50% is deposited thermally.

The opacity of r-process material at the relevant densities and temperatures is not well known. The main contribution to the opacity is presumably due to millions of atomic lines, which are Doppler broadened by the high differential velocities in the ejecta. Unfortunately, complete atomic line lists for these high- Z species are not available. Given the uncertainty, we assume in these calculations a constant gray opacity of $\kappa = 0.1 \text{ cm}^2 \text{ g}^{-1}$ which is characteristic of the line expansion opacity from iron group elements (e.g. Kasen & Woosley 2007). This is in contrast to the work of Metzger et al. (2010b), where oscillator strengths for pure Fe were assumed with ionization potentials from Pb. Considering that neither approach will yield accurate spectral information, we feel that our simple grey opacity scheme is as reasonable an approximation as that used in Metzger et al. (2010b).

We directly calculated the spatial distribution of gamma-ray heating by following the transport of gamma-rays and determining the fraction of their energy thermalized by Compton scattering and photoelectric absorption. Since the dominant Compton opacity has only a weak wavelength dependence, the exact spectrum of gamma-ray emission from the radioactive source does not strongly affect the results. We therefore simply assumed all gamma-rays were emitted at 1 MeV. Before two days, the gamma-ray thermalization rate is greater than 80%.

3. DETAILED PROPERTIES OF THE ELECTROMAGNETIC COUNTERPARTS

In the top panel of figure 3, the R-band light curves for the four models in table 1 are shown. As would be expected from the simple models of Li & Paczyński (1998), the peak luminosity correlates with the total ejected mass of radioactive elements and the time of the peak scales inversely with mass and velocity. Because the total mass ejected in these mergers is not very sensitive to q , the nature of the merger cannot easily be determined solely from the peak time or luminosity. Additionally, the vari-

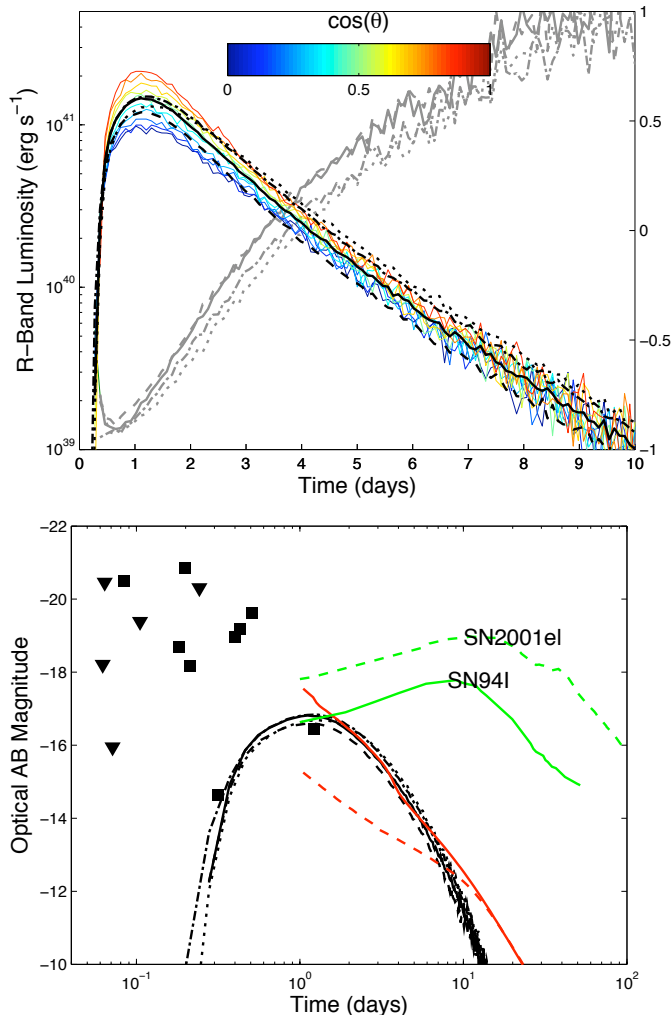


Figure 3. Top: r -band luminosities for the three models described in table 1. The solid lines correspond to the $q = 1.0$ NS-NS merger, the dashed lines to the $q = 0.95$ NS-NS merger, the dotted lines to the $q = 0.88$ NS-NS merger, and the dot-dashed lines to the BH-NS merger. The black lines are the r -band luminosity for the models (left axis), averaged over all solid angles. The gray lines are the $g - r$ color evolution for the models (right axis). The colored lines give the luminosity as a function of polar angle (averaged over the ϕ direction) for the $q = 1.0$ NS-NS merger. Bottom: r -band magnitudes for the same models, along with observed SGRB afterglow absolute magnitudes (filled squares) and upper limits (downward pointing triangles) from the compilation of Berger (2010) where red shifts were obtained. All of the points correspond to separate events. Synthetic SGRB afterglow light curves from van Eerten & MacFadyen (2011) for a jet energy of 1×10^{48} ergs are also shown, where the solid (dashed) red line is for a jet opening angle of 0.2 (0.4) radian. The solid green curve is the optical light curve of SN94I, a type Ic supernova. The dashed green curve is for SN2001el, a type Ia supernova.

ation in peak luminosity with viewing angle within a single model is as large as the variation in the angle averaged peak luminosity between models. This is also shown in figure 3. This further complicates our ability to distinguish between different mass ratios and progenitor models based only on luminosities.⁵

Still, it may be possible to determine if one or two

⁵ We also do not observe the non-smooth structures seen in the light curves of Metzger et al. (2010b), which are due to their use of approximate non-grey opacities.

tails are present based on the color evolution of the light curves. In NS-NS mergers which produce two tails, the luminosity of the transient will be given by the sum of the luminosities of the tails, each of which can be approximated as a Li & Paczyński (1998) expanding sphere. We denote here the heavier and lighter tails with the subscript 1 and 2, respectively. Li & Paczyński (1998) find that at late times, the evolution of the effective temperature is given by $T_{\text{eff}} \approx 4.7 \times 10^3 \text{ K } (M/0.01M_{\odot})^{1/4} (c/v)^{3/4} (\text{day}/t)^{3/4} (f/3 \times 10^{-5})^{1/4}$. The ratio of the effective temperatures in the tails at late times is then

$$\frac{T_{\text{eff},1}}{T_{\text{eff},2}} \approx \left(\frac{M_1}{M_2} \right)^{1/4} \left(\frac{v_2}{v_1} \right)^{3/4}. \quad (1)$$

Significant variation in color from the single tail case is then expected only for a considerable difference between velocities. In this case, tail 2 will shift the total light blueward if it makes an important contribution to the total luminosity at any time. The time of peak luminosity for a single tail is given by $t_m \approx 1 \text{ day } (M/0.01M_{\odot})^{1/2} (3v/c)^{1/2}$. If the velocity of the second tail is much lower, it contributes more to the total luminosity at late times and the light will be bluer compared to the more massive tail emitting radiation alone.

In our detailed models, the velocity difference between the tails is not significant enough compared to the mass difference between the tails in either of the asymmetric NS-NS merger models for the tails to be easily discernible in their color evolution, as shown in figure 3. As a result, there is no significant distinguishing characteristic between ejecta geometries in their colors. All four models show similar reddening as a function of time.

Without knowing the detailed line opacity of the R-process elements, it is difficult to predict the spectroscopic signatures of NS mergers. We expect that high- Z atoms will have a very large number of lines in the optical, similar to and perhaps exceeding the number known for the iron group elements. Because the ejecta velocities in the tidal tails are a factor of $\sim 2 - 3$, larger than ordinary supernovae, the absorption features in the photospheric phase ($\lesssim 15$ days) should be very broad. The likely outcome is a blending together of the lines into a relatively featureless continuum, not unlike the early time observations of broad line Type Ic supernovae (c.f. Galama et al. 1998).

More detailed information about the ejecta geometry could be inferred from spectroscopic observations taken at late times ($\gtrsim 15$ days) when the ejecta has entered the nebular phase and emission features begin to appear. Assuming relatively unblended lines (or line complexes) are present at these epochs, the spectral features should show double peaked emission profiles, at least for equatorial viewing angles. The relative strength of the peaks could be used to estimate the relative masses of the two tails.

In brief, the inclusion of realistic ejecta geometries does not significantly alter the predictions made by simple spherical “tail” models which include realistic nuclear physics. This can be attributed to the fact that the ejecta does not deviate far from a spherical geometry, the relative masses and velocities of the two tails do not induce significant differences in the peak temperatures

of the two tails, and we have assumed a gray opacity. Therefore, we have shown that the uncertainty does not lie in the structure of the ejecta, but in the total ejected mass, its velocity structure, and the opacity of pure r -process material. The ejected mass and velocity are both dependent on the nuclear EoS (Lee 2000; Oechslin et al. 2007) and the treatment of gravity (Rosswog 2005), both of which we have not studied in detail here. Also, heating from r -process nucleosynthesis may effect the dynamics of the material and the total ejected mass (Metzger et al. 2010a). The opacity of pure r -process material has not been studied at these low densities, so its relevance cannot be accurately assessed at this time.

4. IMPLICATIONS FOR SGRBS, GW OBSERVATIONS, AND THE R -PROCESS

If compact object mergers are indeed the progenitors of SGRBs, these optical transients could possibly be seen along side their more spectacular prompt gamma-ray display. In the second panel of figure 3, we compare our synthetic optical light curves to optical afterglow observations and upper limits of SGRBs taken from Berger (2010). Clearly, the optical observations are all for on-axis SGRBs. We also show two synthetic on-axis SGRB optical afterglow light curves taken from van Eerten & MacFadyen (2011), and for comparison, the light curves of two standard supernovae. It seems that the optical observations can be reasonably explained by afterglow models, but, interestingly, they also do not rule out the possible contribution of an r -process powered supernova. It is also expected that in a sizeable fraction of events, these r -process powered supernovae may dominate the optical light at timescales of a day.

The current and next generation of surveys (such as PTF, SASIR, Pan STARRS and LSST) will be sensitive to very subtle changes in flux, for sources with variability timescales of more than a few days, across most of the sky. In table 2, we show the detection rates expected for three transient surveys given the low, recommended, and high merger rates given in Abadie et al. (2010), calculated assuming a cosmology given by Komatsu et al. (2009) and a constant merger rate per volume. The rates are corrected for the effects of a finite cadence.⁶ For the PTF and Pan STARRS, the detection rate is significantly lower than that expected for advanced LIGO whereas the inverse is true for SASIR and LSST. This suggests that, if these large numbers of events are observed, optical observations will be more readily detectable than the associated gravity waves which could help focus gravitational wave searches and better constrain compact object merger rates.⁷ Additionally, we find that LSST will potentially be able to detect these events out to $z > 0.3$, giving a handle on the evolution of the merger rate with cosmic time.

It is clear from this and previous work (Freiburghaus et al. 1999; Goriely et al. 2005) that large amounts of r -process material will be ejected in these events which may contribute significantly to the total r -process budget of the galaxy, although there may be some problems

explaining the low metallicity halo r -process abundance data within this scenario (Argast et al. 2004). Because the production of r -process elements is robust in the tails (i.e. the production of material with $A > 120$ is insensitive to the initial conditions of the material), the major uncertainty in this model lies in the amount of mass ejected in these events and how this material is spread through individual galaxies (Zemp et al. 2009; Kelley et al. 2010). This is in contrast to the other possible site of r -process nucleosynthesis, neutrino driven winds, where the uncertainty lies in finding conditions that make an r -process (c.f. Roberts et al. 2010). For a given amount of mass ejection, the total amount of r -process material in the Milky Way puts an upper limit on the merger rate (Metzger et al. 2010b). Given these considerations, it seems likely that observations, or lack thereof of the transients produced in these mergers will give significant insight into the evolution of r -process material in the Universe.

Useful discussions with C. Fryer and S. Woosley are gratefully acknowledged. LR would like to thank Raph Hix for allowing us to use his nuclear network code and for many useful discussions concerning its use. We acknowledge support from an NNSA/DOE Stewardship Science Graduate Fellowship (LR) (DE-FC52-08NA28752), the University of California Office of the President (LR) (09-IR-07-117968-WOOS), the DOE SciDAC Program (DK) (DE-FC02-06ER41438), CONA-CyT (WHL) (83254, 101958), and the David and Lucille Packard Foundation (ERR) and the NSF (ERR) (AST-0847563). Computing time was provided by ORNL through an INCITE award and by NERSC.

REFERENCES

- Abadie, J., et al. 2010, *Classical and Quantum Gravity*, 27, 173001
- Abbott, B., et al. 2008, *Phys. Rev. D*, 77, 062002
- Argast, D., Samland, M., Thielemann, F., & Qian, Y. 2004, *A&A*, 416, 997
- Berger, E. 2010, *ApJ*, 722, 1946
- Bloom, J. S., et al. 2006, *ApJ*, 638, 354
- Frankel, S., & Metropolis, N. 1947, *Physical Review*, 72, 914
- Freiburghaus, C., Rosswog, S., & Thielemann, F. 1999, *ApJ*, 525, L121
- Galama, T. J., et al. 1998, *Nature*, 395, 670
- Gehrels, N., Ramirez-Ruiz, E., & Fox, D. B. 2009, *ARA&A*, 47, 567
- Goriely, S., Demetriou, P., Janka, H., Pearson, J. M., & Samyn, M. 2005, *Nuclear Physics A*, 758, 587
- Hix, W. R., & Thielemann, F. 1999, *Journal of Computational and Applied Mathematics*, 109, 321
- Hjorth, J., et al. 2005, *ApJ*, 630, L117
- . 2003, *Nature*, 423, 847
- Kasen, D., Thomas, R. C., & Nugent, P. 2006, *ApJ*, 651, 366
- Kasen, D., & Woosley, S. E. 2007, *ApJ*, 656, 661
- Kelley, L. Z., Ramirez-Ruiz, E., Zemp, M., Diemand, J., & Mandel, I. 2010, *ApJ*, 725, L91
- Kocevski, D., et al. 2010, *MNRAS*, 404, 963
- Komatsu, E., et al. 2009, *ApJS*, 180, 330
- Lattimer, J. M., & Schramm, D. N. 1976, *ApJ*, 210, 549
- Lee, W. H. 2000, *MNRAS*, 318, 606
- Lee, W. H., & Ramirez-Ruiz, E. 2007, *New Journal of Physics*, 9, 17
- Lee, W. H., Ramirez-Ruiz, E., & van de Ven, G. 2010, *ApJ*, 720, 953
- Li, L., & Paczyński, B. 1998, *ApJ*, 507, L59
- Mamdouh, A., Pearson, J. M., Rayet, M., & Tondeur, F. 2001, *Nuclear Physics A*, 679, 337
- Metzger, B. D., Arcones, A., Quataert, E., & Martínez-Pinedo, G. 2010a, *MNRAS*, 402, 2771
- Metzger, B. D., et al. 2010b, *MNRAS*, 406, 2650

⁶ Even a cadence of 3 days reduces the detection rate by a factor of two compared to when the effects of a finite cadence are left out.

⁷ We note that even if all compact mergers are associated with SGRBs, the r -process powered SNe will still dominate the off-axis optical afterglow.

Table 2

Detection Rates for Various Blind Transient Searches. Properties of the surveys are assumed to be the same as those given in Strubbe & Quataert (2009).

Model	PTF			Pan STARRS			LSST			SASIR		
	R_{low}	R_{re}	R_{high}	R_{low}	R_{re}	R_{high}	R_{low}	R_{re}	R_{high}	R_{low}	R_{re}	R_{high}
NS-NS	0.1	10	100	1.3×10^{-3}	0.13	1.3	2.3×10^1	2.3×10^3	2.3×10^4	1.2	120	1.2×10^3
BH-NS	7.3×10^{-3}	0.36	12	8.4×10^{-5}	4.2×10^{-3}	0.14	1.6	79	2.6×10^3	0.083	4.1	140

Note. — All rates are in detections per year.

Möller, P., Pfeiffer, B., & Kratz, K. 2003, Phys. Rev. C, 67, 055802
 Nakar, E. 2007, Phys. Rep., 442, 166
 Oechslin, R., Janka, H., & Marek, A. 2007, A&A, 467, 395
 Panov, I. V., Korneev, I. Y., Rauscher, T., Martínez-Pinedo, G., Kelić-Heil, A., Zinner, N. T., & Thielemann, F. 2010, A&A, 513, A61+
 Perley, D. A., et al. 2009, ApJ, 696, 1871
 Rasio, F. A., & Shapiro, S. L. 1994, ApJ, 432, 242
 Rauscher, T., & Thielemann, F. 2000, Atomic Data and Nuclear Data Tables, 75, 1
 Roberts, L. F., Woosley, S. E., & Hoffman, R. D. 2010, ApJ, 722, 954
 Rosswog, S. 2005, ApJ, 634, 1202

Rosswog, S. 2007, in Revista Mexicana de Astronomia y Astrofisica Conference Series, Vol. 27, Revista Mexicana de Astronomia y Astrofisica, vol. 27, 57–79
 Rosswog, S., & Liebendörfer, M. 2003, MNRAS, 342, 673
 Rosswog, S., Ramirez-Ruiz, E., & Davies, M. B. 2003, MNRAS, 345, 1077
 Schenk, O., Bollhofer, M., & Romer, R. A. 2008, SIAM Review, 50, 91
 Shibata, M., Taniguchi, K., & Uryū, K. 2005, Phys. Rev. D, 71, 084021
 Strubbe, L. E., & Quataert, E. 2009, MNRAS, 400, 2070
 van Eerten, H. J., & MacFadyen, A. I. 2011, ArXiv e-prints
 Wahl, A. C. 2002, Systematics of Fission-Product Yields, Tech. Rep. LA-13928, Los Alamos National Laboratory, Los Alamos, N.M.
 Wright, E. L. 2006, PASP, 118, 1711
 Zemp, M., Ramirez-Ruiz, E., & Diemand, J. 2009, ApJ, 705, L186